Solar cell demand for bifacial and singulated-cell module architectures

Nico Wöhrle, **Elmar Lohmüller**, **Max Mittag**, **Anamaria Moldovan**, **Puzant Baliozian**, **Tobias Fellmeth**, **Karin Krauss**, **Achim Kraft** & **Ralf Preu**, Fraunhofer Institute for Solar Energy Systems ISE, Freiburg, Germany

ABSTRACT

The pursuit of achieving higher power output of silicon-based PV modules demands creative improvements in module design in order to reduce geometrical, optical and electrical cell-to-module (CTM) losses. A suitable method, which has been known since Dickson's patent in 1956 (but has been mostly under the radar of the manufacturing industry), is the shingling of singulated solar cell stripes. This technology offers three advantages in comparison to modules with standard-sized solar cells. First, blank cell spacing in the module is minimized, thus increasing the power-generating area per module area. Second, the active cell area is busbar-less, which leads to reduced shading losses. Third, because of the smaller area of the solar cell stripes, the generated current per cell is less, which results in a reduction in the overall series resistance of the cell interconnection within the module. To boost the power output of such a shingled module even further, the introduction of bifacial properties is suggested. To make this bifacial shingled module technology visible on the industry's radar, a practical concept is essential; this paper presents, step by step, Fraunhofer ISE's approach for a bifacial shingled module. Suitable bifacial cell concepts – such as passivated emitter and rear (PERC), passivated emitter, rear totally diffused (PERT), and passivated emitter, rear locally diffused (PERL) – are briefly introduced. The PERL cells are based on the PassDop approach, in which the rear-side passivation layer stack also acts as a doping source during local laser doping. Furthermore, next-generation bifacial cell concepts based on selective and/or passivated contacts, such as in the already established silicon heterojunction technology (SHJ) and the tunnel oxide passivated contact (TOPCon) approaches, developed at Fraunhofer ISE, are presented. Laser-assisted cutting as the singulation technology for realizing the cell stripes, and the challenge of charge-carrier recombination at the cutting edges, are discussed. A bifacial simulation model is presented for the singulated shingle solar cells, covering the question of the impact of different recombination factors, bifacial gains and optimizations of the cell layout. Finally, the module assembly, as well as a detailed calculation of module output power and a comparison with standard module layouts, is presented. This comparison emphasizes the advantages offered by bifacial shingled modules, with the potential to achieve a module power of 400W with a power density of 240W/m² and beyond, for irradiance intensities of 1,000W/m² and 100W/m² from the front and rear sides respectively.

Introduction

The first appearance of a shingled solar cell interconnection pattern (see Fig. 1) dates back to 1956 with a US patent filed by Dickson [1] for Hoffman Electronics Corporation, which is just two years after the first publication of a silicon solar cell by Chapin et al. [2]. In the years that followed, further patents were filed containing concepts of shingling solar cells serving various module designs and applications – for example, Nielsen [3] for Nokia Bell Labs, Myer [4] for Hughes Aircraft Company, Baron [5] for Trw Inc, Gochermann and Soll [6] for Daimler-Benz Aerospace AG, Yang et al. [7] for Silevo LLC, and the most recent patent applications by Morad et al. [8–10] for SunPower Corporation in 2016. Besides the patents, there are a number of items in the literature that have been devoted to this topic in the last few years, with publications by Zhao et al. [11], Glunz et al. [12] and Beaucarne [13]. Recently, the first widely available commercial shingled module was introduced by SunPower [14] as their top-of-the-line product; according to the data sheet, these modules feature a backsheet and are therefore not bifacial.

The idea of singulated solar cells interconnected by a shingling design is therefore by no means new. The early publications of shingling approaches were mostly motivated by particular design requirements, such as modules that were curved, triangular [4] or dome shaped [6]. Later publications started to make use of the potential for achieving

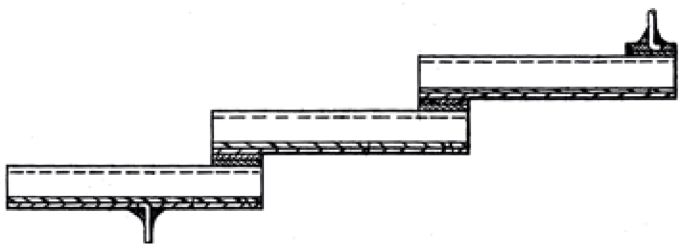

Figure 1. First published illustration of the shingling scheme for monofacial silicon solar cells, taken from Dickson's patent [1] (the descriptive labels in the original image have been removed for reasons of clarity).

higher module power densities with this technique than with standard-module cell interconnection, for example in the limited available space on the vehicle for the 'World Solar Challenge' in 1996 [11]. Consequently, a few large module manufacturers [7,14] seem to have rediscovered the potential of shingling technology to reduce cell-to-module (CTM) losses. The International Technology Roadmap for Photovoltaic (ITRPV) 2017 projects a world market share of 7% for shingled interconnection technology by 2027 [15].

> "The opportunity is at hand for combining bifacial solar cell technology with shingle cell module technology."

Another line of technological evolution spreading in the PV industry is the concept of bifacially illuminated solar cells, which has been extensively covered in a recent article by Kopecek and Libal [16]. As the demand for modules with high power density is large, the opportunity is at hand for combining bifacial solar cell technology with shingle cell module technology, with bifacial cells profiting from additional light coming from the rear side. The busbars on the front and rear sides for the shingle cells are covered by an active area from the adjacent cells, leading to a virtually busbar-free cell string.

The approach for such a bifacial shingle module is presented in three stages. First, eligible bifacial cell concepts – including passivated emitter and rear (PERC [17]), passivated emitter, rear totally diffused (PERT [18]), and passivated emitter, rear locally diffused (PERL [19]) – will be discussed. For this study, the PERL concept is based on the PassDop approach [20–22], in which the rear-side passivation layer stack – i.e. the layer stack consisting of aluminium oxide (AlO_x) and boron-doped silicon nitride (SiN_x:B) – also serves as a doping source for local laser doping. Furthermore, cell concepts with selective and/or passivated contacts that are based on silicon heterojunction (SHJ [23]) or hybrid PERC structures with tunnel oxide passivated contacts (TOPCon [24]) on the rear side will be discussed. Second, physically and technically relevant challenges for the transition from standard cells

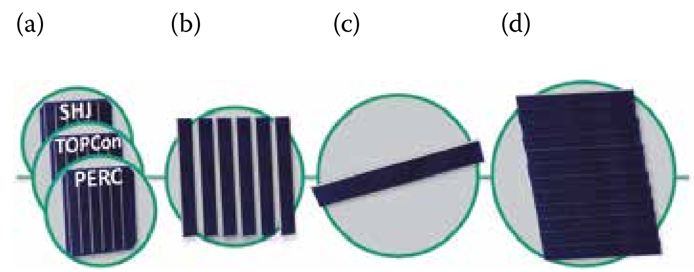

Figure 2. Schematic of the different process steps in the fabrication of shingle modules, starting from bifacial cells on a standard-sized wafer with an edge length of 156mm. (a) Six shingle solar cells are placed on the large-area wafer. The cell concept is modular; silicon heterojunction (SHJ), TOPCon and PERC examples are shown here. (b) The individual shingle cells are singulated into cell stripes. (c) A magnified single shingle cell. (d) Cell stripes are shingled onto each other to form a string.

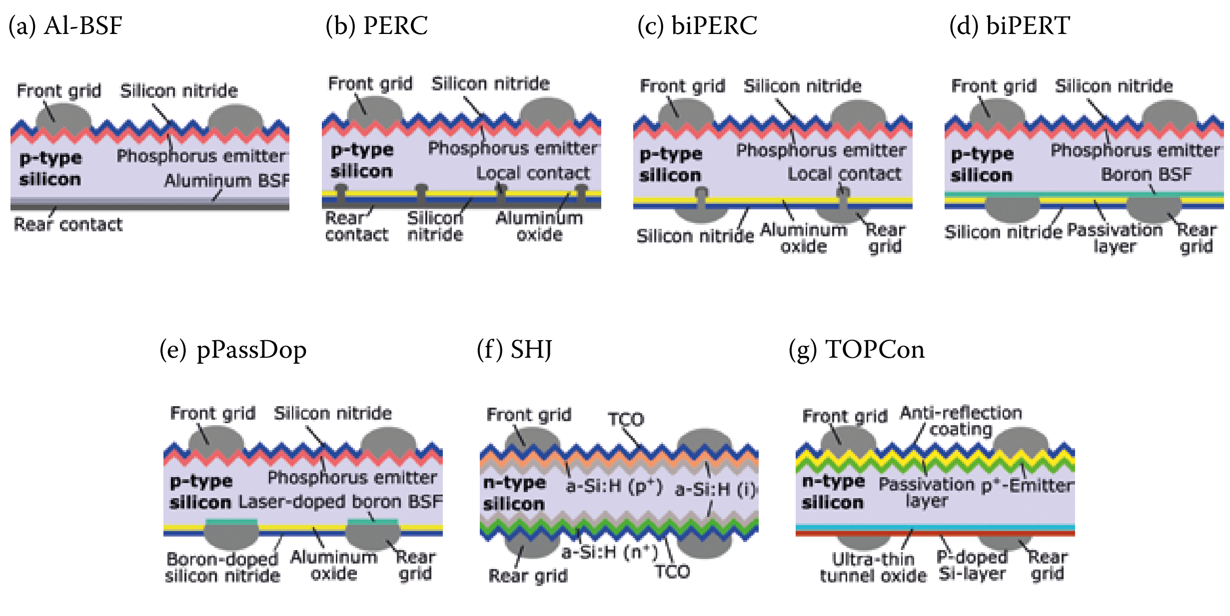

Figure 3. Schematic cross sections of seven different silicon solar cell types with homogeneous emitter. (a) Aluminium back-surface field (Al-BSF) cell. (b) Monofacial PERC with local rear-side contacts. (c) Bifacial PERC with finger grid on the rear side. (d) Bifacial PERT concept with full-area rear-side BSF. (e) Bifacial pPassDop concept with local laser-boron-doped BSF. (f) Silicon heterojunction (SHJ) cell with doped amorphous silicon emitter and a transparent conducting oxide (TCO) as anti-reflection layer. (g) Bifacial TOPCon cell with passivated rear-side contacts (the bifacial rear side shown is only a concept at the moment).

to stripe cells will be addressed, including a discussion of edge recombination effects with a suitable full-cell simulation model realized with the Quokka3 tool [25]. Third, module integration strategies and CTM-loss calculations are provided.

As a name convention, the term 'output power density' P_{out} (mW/cm^2) will always be used instead of 'energy conversion efficiency' η (%) for measurement data referring to bifacial illumination, as that unit is less ambiguous. The scale chosen is such that, with a monofacial irradiation of 1,000W/m^2, the respective numerical values for P_{out} and η are identical.

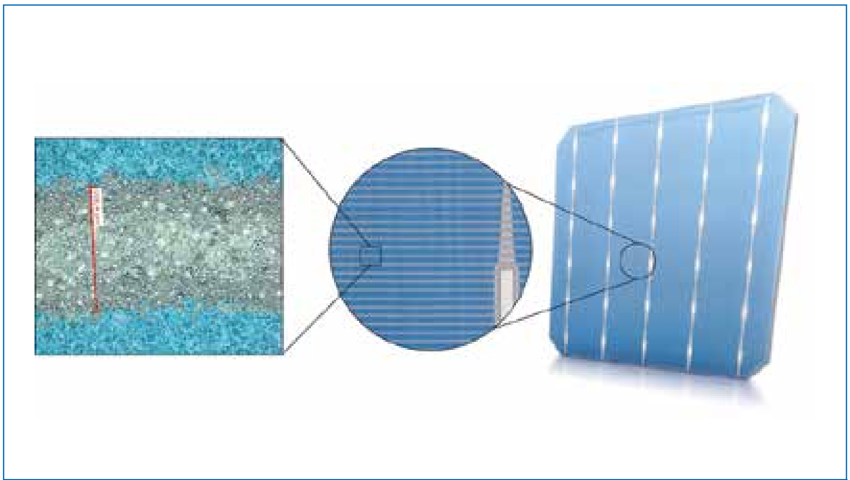

Figure 4. Bifacial PERC solar cell with a screen-printed aluminium rear finger grid with a finger width approaching 100µm [34]. The indicated selection has a measured width of 108.4µm, while the underlying LCO features a width of 30–35µm.

Approach

To achieve a module output power P_{module} of 400W with power densities of 240W/m^2 and beyond for a standard 60-cell module with a size of 1.68m × 1.00m (irradiation intensities of 1,000W/m^2 and 100W/m^2 from the front and rear sides respectively), the approach proposed here is to apply shingling technology in order to use the module area as efficiently as possible. By shingling the solar cells, three CTM-related types of loss are minimized, namely 1) losses due to inactive module area; 2) shading losses due to busbar contacts; and 3) series resistance losses due to cell interconnection. To also benefit from the additional rear-side illumination from bifacial solar cell architectures, the proposed shingle solar cell and module technology is also bifacial in nature. The authors foresee a large potential for this bifacial shingling approach in cases where the 'old idea' of shingled modules can be merged with state-of-the art bifacial solar cell concepts.

To raise interest with regard to industrial mass production, standard-sized solar cell manufacturing sequences, with only minor adaptations, should be utilized for the manufacturing of shingle solar cells. Thus, the most obvious industrial solar cell concept to be used is the bifacial passivated emitter and rear cell (biPERC) technology, utilizing p-type Czochralski-grown silicon (Cz-Si) wafers. Fig. 2 illustrates four different typical stages of the fabrication of shingle solar cells and module strings, starting from a standard wafer with an edge length of 156mm. The general approach here is to create a certain number (six in this example) of shingle solar cells on a large-area wafer.

After metallization and contact formation, the cell stripes are singulated by a laser-assisted cutting process. Subsequently, the single cell stripes are interconnected by shingling the cells onto each other. Since singulation into stripe cells results in an increased contour-to-area ratio, edge passivation becomes important and needs to be considered. This design approach will be called the *shingled passivated edge, emitter and rear (SPEER)* solar cell concept. A true indication of strength of the module assembly of shingle cells is the modularity of the chosen cell concept to be utilized; the shingle module concept can therefore directly profit from progress in solar cell efficiency, while keeping the same module platform, and thus the same module manufacturing process.

Apart from the SPEER solar cells (which can be based on PERC, PERT or PERL structures), approaches with passivated contacts (SHJ, TOPCon) are within the scope of the work currently being pursued at Fraunhofer ISE. The shingle solar cells that are based on passivated contact approaches are called the *shingled passivated edge, emitter, rear and contact (SPEERCon)* solar cell concept.

Eligible bifacial cell concepts

At the moment, aluminium back-surface field (Al-BSF) solar cells (see Fig. 3(a)), with a market share of around 80% in 2016 [15], still dominate the industrial production of crystalline silicon solar cells. However, the passivated emitter and rear cell (PERC) [17] (see Fig. 3(b)) allows higher energy conversion efficiency as a result of its dielectrically passivated rear side. The market share for PERC has gradually increased, to about 15%, in the last few years, and is expected to win significant market share over Al-BSF technology in the future [15]. Besides the dielectric rear-side passivation, one of the main features distinguishing PERC from Al-BSF cells is the local contacts on the rear side. On the Fraunhofer ISE PV-TEC pilot line [26], the baseline PERC process has yielded energy conversion efficiencies of 21.0% to 21.5% on p-type Cz-Si with a homogeneous emitter and a 156mm edge length [27–29].

A bifacial solar cell can harvest additional light coming from the rear side (depending on albedo) [16], if an appropriate module concept, such as a glass-glass module, is used. Bifacial cell and module technology therefore offers a higher energy yield potential in cases where the energy conversion efficiency of the front side of the cells is not significantly influenced by the bifacial approach, and is thus on a similar level to their monofacial cell counterparts. Hence, reducing the metallized rear-side area from a full-area metallization, as commonly employed for PERC cells, to a metallization grid is a logical technological adaptation (Fig. 3(c)). With a metallization grid on the rear side instead of a full-area metallization, the bifacial application is enabled, and the adapted cell structure is referred to as *biPERC*.

The potential of PERC-like bifacial cell architectures was shown on cells in the laboratory back in the 1990s [30–32]. Industrial large-area p-type biPERC cells with a screen-printed aluminium rear-side grid were first realized on multicrystalline silicon in 2016, achieving an efficiency of η = 17.8% [33]. Subsequently, biPERC solar cells utilizing p-type

Cell type	Cell area [cm^2]	Material	Finger width rear side [µm]	Monofacial illumination	V_{oc} [mV]	j_{sc} [mA/cm^2]	*FF* [%]	η_{mean} [%]	η_{max} [%]	Bifaciality factor [%]
biPERC*	243	p-type Cz-Si	100	Front	660	39.5	79.3	20.7	20.7	76.8
				Rear	654	30.7	79.6	15.9	16.4	
			150	Front	660	39.5	79.8	20.8	20.9	72.1
				Rear	652	28.8	80.1	15.0	15.5	
			200	Front	661	39.5	79.9	20.9	21.0	66.0
				Rear	651	26.6	80.3	13.8	14.2	
Monofacial PERC*			–	Front	656	39.8	80.0	20.9	21.1	–
biPERT*	243	p-type Cz-Si	200	Front	654	39.5	79.3	20.4	20.5	68.1
				Rear	642	26.1	79.9	13.9	13.9	
			50	Front	635	39.2	79.7	19.8	19.9	86.4
				Rear	632	33.7	80.3	17.1	17.2	
Monofacial PERT*			–	Front	656	39.8	80.0	20.9	21.1	–
pPassDop*	244	p-type Cz-Si	65	Front	638	39.1	79.4		19.8	88.9
				Rear	635	34.6	79.8		17.6	
Monofacial TOPCon*	4	n-type FZ-Si	–	Front	725	42.5	83.3		25.7	–
Bifacial SHJ†	244	n-type FZ-Si	50	Front	738	38.9	81.5		23.4	93.6
				Rear	738	35.7	83.2		21.9	

* Fraunhofer ISE solar cells; † Meyer Burger solar cells

Table 1. Open-circuit voltage V_{oc}, short-circuit current density j_{sc}, fill factor *FF*, energy conversion efficiency η, and bifaciality factor η_{rear}/η_{front} for various solar cell groups.

Cz-Si have been reported to achieve conversion efficiencies of up to η = 21.0% [34,35] (measured on a black non-conductive chuck). Beyond enabling the bifacial application, a further advantage of biPERC solar cells compared with PERC cells is a reduced consumption of aluminium paste.

When the full-area rear metallization is reduced to an aluminium grid with thin finger contacts, there are challenges associated with aligning the laser contact opening (LCO) and with the screen-printing step. Fig. 4 shows the rear view of a screen-printed aluminium finger grid, with finger widths approaching 100µm and a successful alignment with the underlying LCO. In this case, the rear features a very smooth surface, typical of monofacial PERC devices. The rear capping layer thickness has been reduced in order to serve as an anti-reflection coating, although it has not yet been fully optimized, as can be deduced from its optical appearance.

Table 1 shows the current–voltage (*I*–*V*) parameters for monofacial illumination, measured with contact bars on a black non-conductive chuck, of different solar cells featuring different rear-side finger widths. The results for optional monofacial reference cells are also shown for comparison. The monofacial reference for the biPERC cells features a thicker rear capping layer and a full-area aluminium metallization serving as a reflector, increasing the optical generation and thus the short-circuit current density j_{sc}. The biPERC cells feature a reduced capping layer thickness that serves as an anti-reflection coating. As can be seen, the bifacial and the monofacial cells achieve similar efficiency levels of around 21%, where lower j_{sc} and *FF* for the bifacial cell are compensated by V_{oc} gains. The higher V_{oc} is due to the lower recombination-active local contacts for the line-shaped aluminium fingers than in the case of full-area aluminium metallization [36]. By reducing the finger width from 200µm to 100µm, the mean front efficiency η_{front} drops moderately, from 20.9% to 20.7%, as a result of an increased finger resistance. In contrast, the mean rear efficiency η_{rear} increases significantly, from 13.8% to 15.9%. The bifaciality factor, defined by the ratio of η_{rear} and η_{front}, hence increases from 66.0% to 76.8%.

Compared with a biPERC device, the bifacial passivated emitter, rear totally diffused (biPERT) solar cells exhibit a full-area BSF on the rear side; the idea here is to exploit the additional conductivity by increasing the separation of the contacts (Fig. 3(d)). In the case of a p-type base, the presence of the BSF reduces the need for heavy base doping; in consequence, a lighter-doped material, which is less prone to light-induced boron–oxygen-related degradation, can be used. Moreover, the BSF enables the use of alternative pastes for the rear contact, for example silver-aluminium or even pure silver pastes, the latter typically being used for front-side contacts on phosphorus-doped emitters.

Recent developments have put the PERT approach back into the spotlight. Chemical vapour deposition (CVD) technology enables the application of a borosilicate glass (BSG) layer and a capping layer prior to the conventional tube furnace diffusion in a $POCl_3$ atmosphere. During this (co-)diffusion process [36–38], both the BSF and emitter are formed. Furthermore, the remaining rear stack of BSG and capping remains on the wafer, acting also as a passivation and anti-reflection layer. The use of firing-through pastes means that LCO prior to metallization can be omitted, thus also removing the need for alignment between the laser and screen printer.

The biPERT section in Table 1 shows the *I*–*V*-related parameters obtained by exploiting the benefits of co-diffusion. The base doping of these cells is of the order of 4Ωcm, showing that light-induced degradation due to boron–oxygen complexes is significantly reduced. The cells are fully solderable and resemble the appearance of the biPERC cell shown in Fig. 4. Because of the thinner rear-side fingers with biPERT, higher bifaciality factors (in this example 86.4%) can be achieved than with biPERC.

One of the first proofs-of-concept for the 'pPassDop' PERL approach on solar cells with an edge length of 156mm yields η_{front} = 19.8% [39] (see Fig. 3(e) and Table 1). This solar cell achieves a high bifaciality of about 89% because of the rear-side grid with thin contact fingers of only around 65µm in width. The applied 'pPassDop' layer stack consisting of AlO_x/SiN_x:B on the cell's rear side serves as both surface passivation and doping source. Laser processing is used to locally introduce boron atoms from the 'pPassDop' layer stack into the silicon, which results in a boron-doped BSF underneath the rear screen-printed and fired contacts. A special alignment procedure ensures that the rear grid with finger widths of about 65µm is placed over the entire wafer on top of the ~40µm-wide laser-doped and opened lines.

Silicon heterojunction (SHJ) technology (Fig. 3(f)) is also a promising candidate because of its already bifacial design (bifaciality factors above 90%), excellent passivation quality, and high-efficiency potential of up to 25.1% for lab-scale solar cells [40]. Large-area bifacial SHJ cells (with busbar-less metallization) are available on the market, with efficiencies of up to 23.4% [41], and can thus also serve as a candidate for stripe cells. To close the efficiency gap between PERC-like structures and SHJ while maintaining low-cost processing, next-generation hybrid PERC structures with tunnel oxide passivated contacts (TOPCon) are already being developed on lab-scale solar cell sizes with an optional bifacial design; the design concept is illustrated in Fig. 3(g). The monofacial TOPCon cells currently achieve record efficiency values of 25.6% on a lab scale [42]. The TOPCon approach is currently being transferred to large-area wafers and a bifacial structure, and is expected to be market ready in the near future.

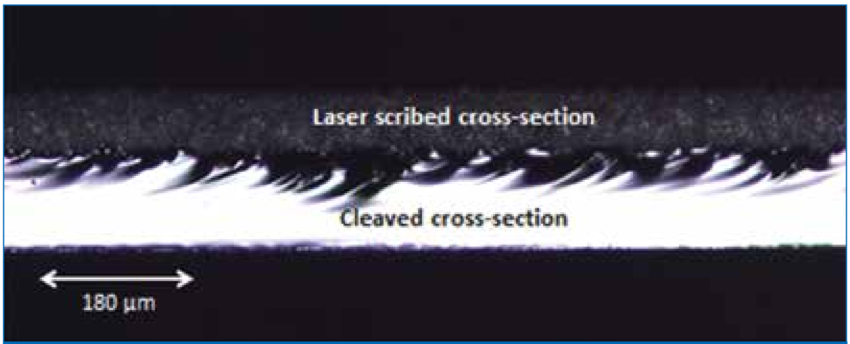

Figure 5. A light-microscope image of a laser-scribed and mechanically cleaved edge of a silicon solar cell.

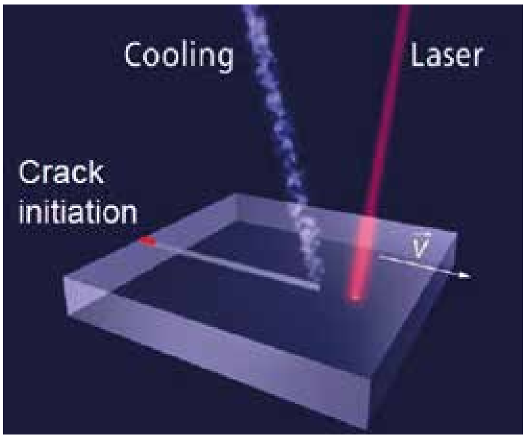

Figure 6. An illustration of the TLS process, showing the crack initiation, laser heating and fluid cooling steps leading to the substrate separation. (Image taken from Lewke [45].)

	Contour/area [1/cm]	$j_{02,edge}$ [nA/cm^2]
25 × 156mm^2 stripe	0.93	12.1
50 × 156mm^2 stripe	0.53	6.9
156 × 156mm^2 cell	0.26	3.3

Table 2. Example calculations for contour-to-area ratio and resulting $j_{02,edge}$ (after Dicker [47]), showing that a 25mm-wide stripe has a fourfold influence on $j_{02,edge}$ recombination, compared with a regular square cell (in the case of an unpassivated edge).

	S_{eff} [cm/s]	$j_{02,edge}$ [nA/cm]
Unpassivated edge	10^6	13
Passivated edge	10	0

Table 3. Applied recombination levels for the cell edges, representing unpassivated and passivated edges.

Technology-specific challenges

Despite the solar cell concepts for shingling technology being quite diverse, they will all face the separation process step, the potential need for edge passivation, and finally the integration into a module.

Separation

The quality of the separation of the solar cell stripes is closely related to edge recombination, as the separation process may induce damage to the edge and leaves a surface with a process-dependent damage density and roughness. In the case of SPEER and SPEERCon cells, edge recombination becomes significant because of the high contour-to-area ratio (see next section). The most common method used so far for silicon solar cell separation has been laser scribing, followed by mechanical cleavage [12]. For example, the pulsed laser source engraves about one-third of the cell thickness (usually from the rear side) in the scribing phase [43]; the complete separation of the rest of the solar cell occurs mechanically in the final cleaving step. Fig. 5 shows an example of a cross section of an edge to illustrate the difference in the surface morphology remaining in the scribed and cleaved areas.

Recently, with the increase in half- and quarter-cell production demand [15], thermal laser separation (TLS) [43,44] was proposed as a candidate for future silicon substrate dicing [44]. TLS is a kerf-free, laser-based dicing technology that is based on crack guiding by means of thermally induced mechanical stress [43] (see Fig. 6). This technology is widely used in the semiconductor industry [44]. Briefly, TLS is a two-step process [43], starting with an initial scribe (less than 50μm deep) using a laser source to induce a crack. The second step is the crack guidance. The laser-induced substrate heating creates a compressive stress, followed by a subsequent fluid cooling, which incites tensile stress.

The TLS method of separating silicon wafers has been reported to show a higher edge quality; in initial TLS tests performed on PERC solar cells to obtain half-cells it has been found that this method leads to improved electrical and mechanical properties compared with conventional laser-scribed and cleaved half-cells [44,45]. There have been statements to the effect that the half-cells separated by the TLS process have shown a 1%$_{rel}$ reduction in maximal power, whereas the half-cells separated by conventional laser scribing and cleaving have shown a 1.2%$_{rel}$ power reduction.

To gain a deeper understanding of the TLS parameters [43,44] and their effects on the quality of the edges of the separated stripe cells, further development within the PV production research community is expected. An optimized process should be aimed at creating a very smooth surface as a good basis for subsequent passivation. The introduction of such a laser process into the process chain for the separation of the cell stripes could decrease the recombination of the stripes' edge regions, which will be discussed in the next section.

Edge passivation

As mentioned in the previous section, the singulated solar cell stripes have a larger contour-to-area ratio than standard (pseudo-)square cells, which is illustrated in Table 2 for 2.5cm- and 5cm-wide stripes. Moreover, (pseudo-)square cells undergo a passivation process which also covers the edges, while the stripes are singulated after metallization and contact formation, leaving the edges initially blank. This poses the question of potential losses through recombination at those edges, which can be divided into three subregions:

1. Surfacing bulk region, implicating ideal surface recombination (ideality factor n = 1). This can be accounted for with modelling by using an effective surface recombination velocity between $S_{eff} \approx$ 8cm/s for excellent passivation (e.g. reported by Saint-Cast et al. [46]) and S_{eff} = 10^6cm/s for an unpassivated surface (with high defect density, reported by Glunz and Dicker [12,47]).
2. Surfacing heavily doped emitter region, implicating ideal surface recombination.
3. Surfacing space charge region (SCR), implicating non-ideal surface recombination activity (ideality factor $n \approx$ 2). Dicker parameterized this recombination for a single recombining edge using the second diode in the two-diode model, naming it $j_{02,edge}$ [47]. This recombination current density comprises a determined constant of 13nA/cm scaling with the contour-to-area ratio, so that $j_{02,edge}$ = contour/area·13nA/cm^2. A very similar value has been recently found by Fell et al. [48]. This yields the $j_{02,edge}$ values given in Table 2 for the example stripes.

Figure 7. 3D model of a bifacial SPEER solar cell.

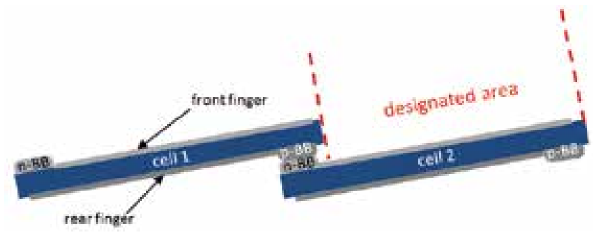

Figure 8. Shingling scheme of two solar cells, whereby the bottom busbar of cell 1 is placed onto the top busbar of cell 2.

For the examined cells, Dicker [47] concluded that the surfacing bulk region recombination and the SCR recombination contribute equally to the total edge recombination, whereas the emitter region surface recombination has a negligible influence because of its small extent.

In the particular case presented here, it is desired to calculate the worst case of all four edges of the stripe cell being recombination active. To model these effects, the newly developed Quokka3 tool (currently in beta stage, with release planned in 2017) will be used. Because a lumped skin approach (an expression originally coined by Cuevas et al. [49]) is used for non-neutral regions, the mesh fineness can be reduced to a minimum. In consequence, this allows the modelling of much larger domains, in this case an entire cell stripe, resulting in a generalized model without spatial simplifications such as potential or series resistance distributions (as opposed to the usual one-cell approach). With the

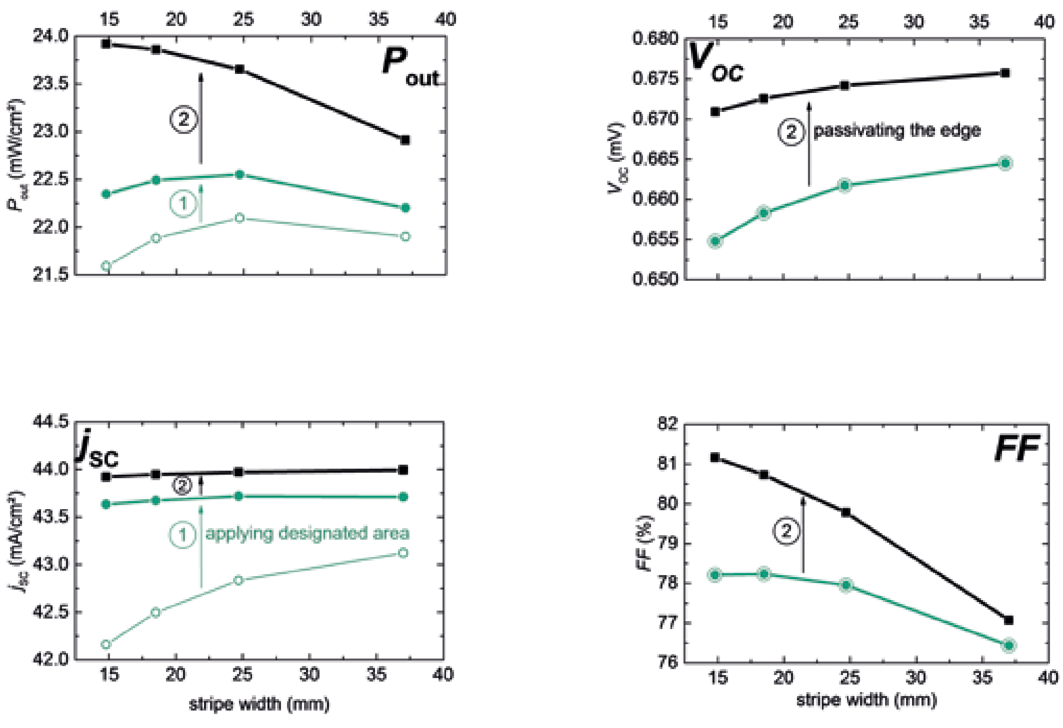

Figure 9. Simulated *I–V* parameters of the stripe cells for various cell stripe widths, for illumination intensities of 1,000W/m² and 100W/m² on the front and rear sides respectively. The lower light-green plot shows the parameters for the full stripe area calculation with maximum recombination at the edges. In step 1, j_{sc} is calculated only for the designated area (see Fig. 8), which excludes the busbar adjacent area because it is covered by the next shingle cell in the module layout. Step 2 includes an excellent edge passivation.

latest addition of a vertical resistance and full injection dependence on the skin parameterization [25], the skins can be described by lumped parameters without errors, compared with, for example, explicitly accounting for doping profiles. The cell stripe CAD model is depicted in Fig. 7.

> "The goal of the cell optimization is to find the ideal cell stripe width and determine the impact of edge recombination."

The input parameters are extracted from a bifacial PERC solar cell that has been processed on the Fraunhofer ISE PV-TEC pilot line, yielding a front-side efficiency of 21% under 1,000W/m² AM1.5g illumination and with a bifaciality of 75% (see Table 1); these parameters are then applied to the stripe cell, which is based on the same processes. The goal of the cell optimization is to find the ideal cell stripe width and determine the impact of edge recombination. Three scenarios are therefore simulated while varying the stripe width, beginning with a stripe cell with a highly recombinational edge (S_{eff} and j_{02} as shown in Table 3).

As shown in Fig. 8, the busbar, as well as the adjacent area, is covered by an active area of the overlying cell; thus, only the marked designated area is relevant in the determination of the j_{sc}. In step one ('1' in Fig. 9), this effect due to shingling in the module is included in the simulated I–V parameters. The second step ('2' in Fig. 9) introduces an excellent edge passivation, assuming S_{eff} = 10cm/s and $j_{02,edge}$ = 0nA/cm. All the results shown were calculated for a bifacial illumination with a front irradiance of 1,000W/m² and a rear irradiance of 100W/m² (which is presumed to be a candidate for a coming standard for bifacial I–V measurements).

Step 1 has a major effect on j_{sc}, but the dependence on the stripe width vanishes as the continuous shading of the busbar is diminished. Moreover, j_{sc} shifts by around 1mA/cm², to 43.7mA/cm², which reflects one aspect of the advantages of shingling technology. Step 2, the edge passivation, manifests its effect mainly in FF and V_{oc}. Reduced SCR recombination at the edges $j_{02,edge}$ leads to a jump in FF by 2–3%$_{abs}$ for small stripes; the reduced base edge recombination S_{eff} increases V_{oc} by 10–15mV for small stripes. Both effects are pronounced for small stripes as a result of their higher contour-to-area ratio.

Step 1 increases the overall power output P_{out} of the stripe cell from 22 to 22.5mW/cm² at an ideal stripe width of 25mm, and reduces the sensitivity to variations in stripe width. Step 2 increases P_{out} to 23.6mW/cm² at a stripe width of 25mm. It increases further with smaller stripe widths, but this is not a suitable approach for cell interconnection, as will be shown in the next section. Overall, with a gain of more than 1mW/cm² it is well worth considering an additional process step for edge passivation. The implementation of such an edge passivation technique, which is in the best case also suitable for mass production, is currently a high-priority line of investigation in the ongoing work at Fraunhofer ISE.

Module integration and CTM loss analysis

As described above (see Fig. 8), the electrical interconnection of solar cells in shingled modules is achieved by overlapping and directly connecting the n and p sides of adjacent solar cells. To increase electrical performance, an electrically conductive adhesive (ECA) or solder paste may be used between the cell stripes [13]. The depth of the overlap is observed to be between 1 and 2mm. A trade-off in overlap between manufacturing requirements (cell lay-up

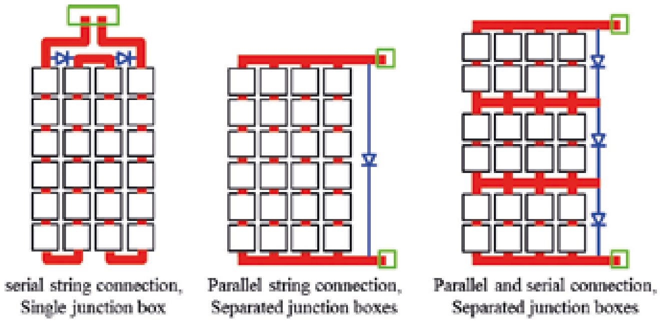

Figure 10. Different module topologies with serial, parallel and combined string interconnection, and single and separate junction boxes.

precision) and costs (shaded cell parts do not generate power, but still have to be purchased) needs to be examined, which is crucial for the module's power/price ratio. The same argument is valid for the size of the shingled cells: although smaller cell stripes decrease some electrical losses because of lower current generation, as shown in the previous modelling, they increase manufacturing requirements, the proportion of overlapped area, and edge recombination losses.

Since all cells are directly connected, a string of significant length without gaps or compensating

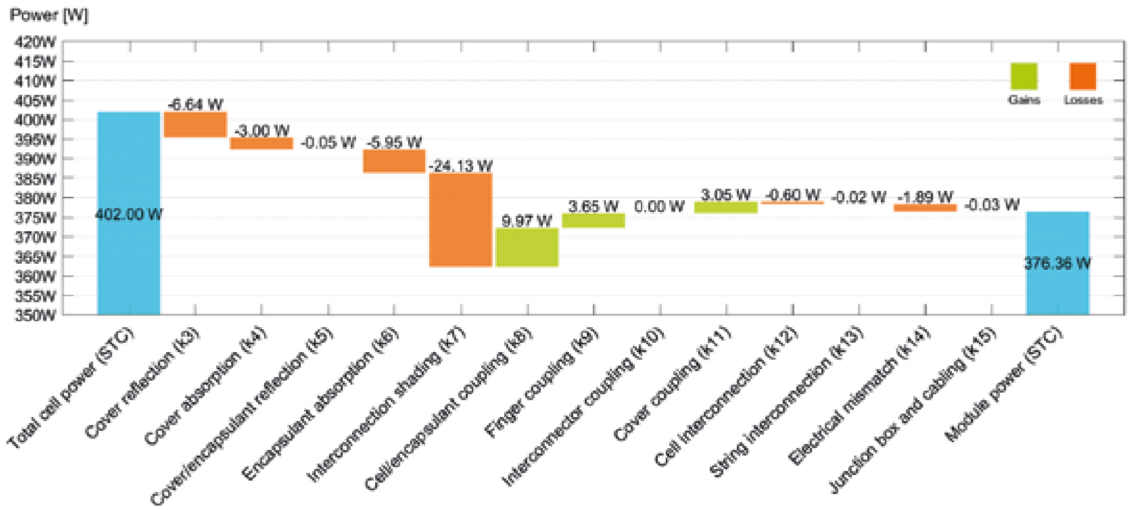

Figure 11. CTM analysis for a shingled module with bifacial PERC cells.

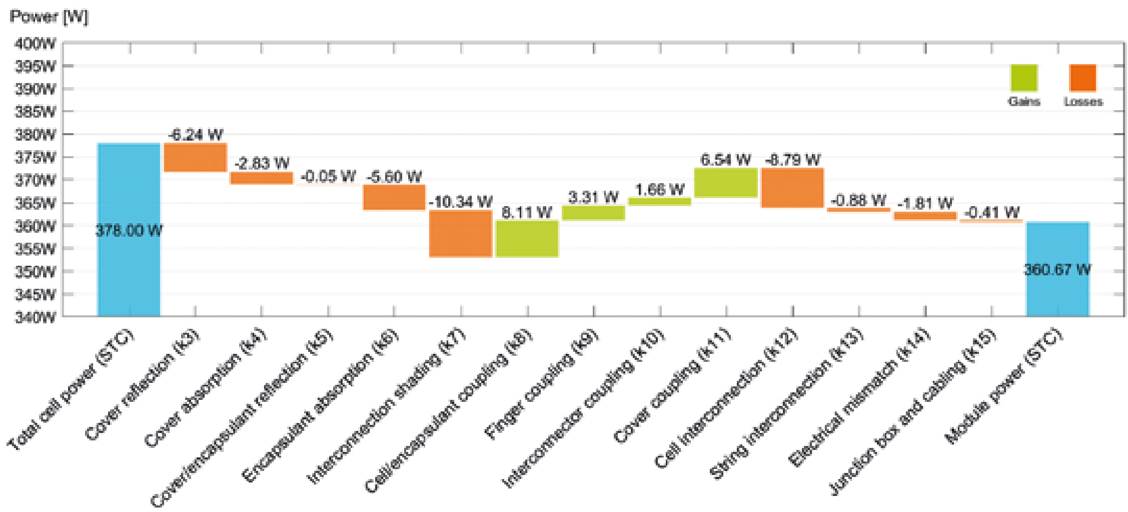

Figure 12. CTM analysis (power) for a conventional module using biPERC solar cells.

elements is formed. At changing temperatures, thermomechanical stress occurs within the cell interconnection and the cell metallization. While the stress from external loads (e.g. snow) may be reduced by placing the solar cells in the neutral plane of double-glass modules, the thermomechanical stress resulting from different coefficients of thermal expansion cannot be avoided.

The direct overlapping of the cell stripes eliminates the cell gaps, and therefore increases the active module area proportion. Two options are possible to take advantage of the resulting gains: 1) reduce the module size, keeping the module power constant and saving on module area and materials; or 2) keep the module area constant and increase power and efficiency. For typical set-ups, either approximately 9% more power than a conventional module can be generated, or the module area can be reduced.

As a result of the increased number of (smaller) solar cells in shingled modules, the module voltage increases if a conventional module topology that connects strings of solar cells in series (Fig. 10) is used. To be compatible with existing inverters, and so as not to exceed electrical limitations, electrical properties similar to conventional PV modules are desirable. New module topologies featuring strings connected in parallel, or using combinations of parallel and serial cell and string interconnection, are therefore necessary and have been discussed in the literature [8,50,51]. Shingling requires new solutions for string interconnection, junction boxes and bypass diode placement.

"Shingling requires new solutions for string interconnection, junction boxes and bypass diode placement."

Shingled modules are a concept that is certainly capable of producing increased module efficiency and module power. A detailed CTM analysis using SmartCalc.CTM by Fraunhofer ISE [52] (also presented in another article in this issue of *Photovoltaics International*, p.97) reveals important gains and losses as well as several major differences with conventional modules.

First, a few remarks on the CTM-loss calculations have to be made. Shingling is the only crystalline module concept in which the active cell area may be shaded by another active area. The overlapping cell area usually has a higher efficiency, since the overlapped cell area features metallization patterns for interconnection.

Let us assume that two cells of the same power are completely overlapped, and that the lower cell is fully shaded and therefore produces no electrical power. Now, only one 'power unit' remains after this overlapping. Since the reference area has also changed, the efficiency remains the same ($CTM_{efficiency}$ = 1). Because initially (before overlapping) two power producing cells were present, the CTM factor for *power* has changed and is now CTM_{power} = 0.5. With shingling, therefore, the CTM factors for power and efficiency do not correspond as they do with other module concepts.

Usually, the absolute power loss is higher for a shingled module than for a conventional one, but so is the sum of the initial cell powers, since more cells are needed to cover the module and the overlapping areas. Figs. 11 and 12 illustrate the higher absolute CTM losses for shingled modules. Nevertheless, shingled modules are capable of achieving higher module powers and efficiencies than conventional modules [53].

Shingled modules do not include interconnection ribbons; thus, there are no electrical losses associated with ribbons, but contact and bulk resistance losses in the ECA occur. Optical gains and losses remain practically unchanged from those of conventional modules, with the exception of backsheet reflections (k11) and potential reflective gains from interconnection ribbons (k10). Electrical mismatch losses are heavily dependent on the manufacturing equipment and the homogeneity of the cell stripes [54].

SmartCalc.CTM was used to analyse the CTM ratio of a shingled module using the modelled bifacial PERC cells described above; results of the analysis are shown in Fig. 11. The module features six strings of 67 shingled cells with dimension 25mm

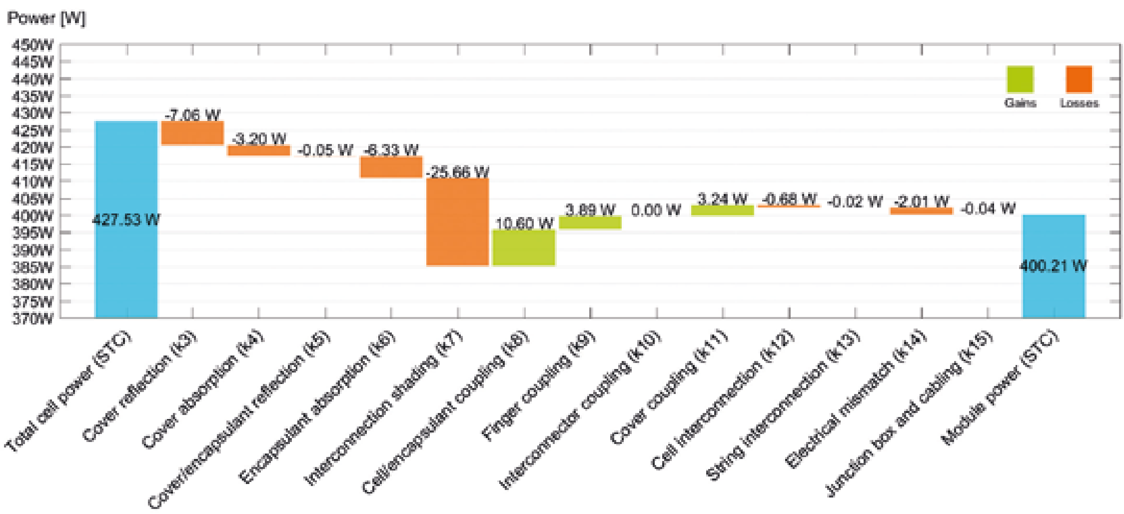

Figure 13. CTM analysis (power) for a shingled module with 400Wp (257W/m²).

× 156mm. Each cell has a power of 1W (P_{out} = 23.2mW/cm² at 1,000W/m² front-side and 100W/m² rear-side irradiance), which corresponds to the black line in Fig. 9 at 25mm, calculated using a full area instead of a designated area. Commercially available module materials – such as EVA, AR-coated glass and a polymer backsheet – are used. The overlap of the cells is set to 2mm; reducing this value would greatly reduce the total power loss from cell to module, but not the final module power. A module with SPEER cells would produce 376W (P_{out} = 21.9mW/cm²).

Full-size biPERC solar cells were used in a conventional module set-up (H-pattern, ribbon interconnection, 205mm pseudo-square, 6W per bifacial cell), and a comparative CTM analysis of both module concepts was performed. Results of the ribbon-interconnected PERC cells are shown in Fig. 12. A conventional ribbon-interconnected module – featuring solar cells with the same biPERC technology as the previous SPEER cells – would only produce 361W.

Since an overlap of the shingled cells of 2mm was chosen, a larger number of cells is necessary for the shingled module (402Wp, Fig. 11). At this point, cost considerations become important and further module optimization is supported with SmartCalc.CTM.

To obtain a module power with the conventional module set-up that is similar to the power that can be achieved with the shingle concept, an increase in the initial cell performance is necessary for H-pattern biPERC cells. Bifacial H-pattern cells with 24.2mW/cm² at 1,100W/m² irradiance (an increase of 1.0mW/cm² compared with the SPEER cells for shingling) would be required to also achieve a module power of 376W. As the approach here features stripe cells based on the specific process technology for large-area cells, the power of the shingled module will automatically surpass that of the conventional module technology by around this margin, even if the cell efficiencies improve.

The next step to reaching the target of 400W per module (at an area of a common 60-cell module) is to perform an estimation of the necessary cell power to achieve this goal. A detailed CTM analysis is shown in Fig. 13.

A parameter sweep of the electrical cell characteristics reveals that SPEER cells with 1.06Wp (P_{out} = 24.7mW/cm²) are required if a shingled module set-up as described above is used. Dividing that output power by 1.1 (irradiance factor), and neglecting the bifaciality factor, the approximate front-side efficiency for such a cell would be η = 22.5%. This is a number which, according to the ITRPV roadmap [15], is to be expected for mass-cells produced by 2021, and has in fact already been achieved for full-size pseudo-square PERC record cells ([55], η = 22.61%). Furthermore, if the next-generation cell concepts discussed above, such as SHJ, are integrated in shingled modules, then powers exceeding 400W in standard-size modules can definitely be expected.

Summary

PV modules with shingled cell technology have a history almost as old as the silicon solar cell itself. With bifacial PERC or PERC-like solar cells, industrially available concepts are at hand that now put shingling technology into an attractive position. A cost-effective cell concept can be boosted by the bifacial shingled module concept towards achieving the module power benchmark of 400W, for a conventional ('60-cell') module size with 1,000W/m² front and 100W/m² rear irradiance, by reducing CTM losses and benefitting from bifacial irradiance gains.

Some of the challenges faced on the path to realizing a bifacial shingled module have been highlighted:

1. Achievement of a monofacial cell efficiency of 22.5% (standard test conditions, 1,000W/m² irradiance) in mass production, which is supposed to be reached by PERC/PERT/PERL R&D in the next two years as a result of industry self-interest.

2. Provision of suitable cell separation techniques and/or reduction in edge recombination through appropriate passivation methods.

3. Development of reliable shingled cell interconnection and precise module assembly to guarantee durability and minimum mismatch in the module.

> "It is the authors' belief that the combination of shingling and bifacial technology offers the greatest and most accessible levers for power output increases in solar modules."

The modularity of the shingling module concept, together with the availability of the presented hybrid PERC (TopCon) or silicon heterojunction concepts, furthermore implies the possibility of even higher module powers, which are basically a bonus when the module concept for biPERC has been developed. Overall, this is encouraging in the development of a product suitable for the industrial and consumer markets, because it is the authors' belief that the combination of shingling and bifacial technology offers the greatest and most accessible levers for power output increases in solar modules. The recent appearance of the first shingled modules from large manufacturers seems to support the considerations discussed in this paper.

Cell Processing

Acknowledgements

The experiments in this work were conducted within the framework of the 'PV-BAT400' project (Contract No. 0324145), supported by the German Federal Ministry for Economic Affairs and Energy. The authors would like to thank all the people in the PMZ, PTQ and SEC teams at Fraunhofer ISE for their support and making this study possible.

References

[1] Dickson, D.C., Jr. 1960, "Photovoltaic semiconductor apparatus or the like", US Patent 2938938 (May 31).

[2] Chapin, D.M., Fuller, C.S. & Pearson, G.L. 1954, "A new silicon p-n junction photocell for converting solar radiation into electrical power", *J. Appl. Phys.*, Vol. 25, No. 5, p. 676.

[3] Nielsen, R.J. & Leif, R. 1963, "Satellite solar cell assembly", US Patent 3116171 (Dec. 31).

[4] Myer, J.H. 1968, "Photovoltaic generator", US Patent 3369939 (Feb. 20).

[5] Baron, W.R. 1969, "Solar cells with flexible overlapping bifurcated connector", US Patent 3459597 (Aug. 5).

[6] Gochermann, H. & Soll, J. 1996, "Shingle-type solar cell generator prodn. – allowing formation of curved or domed product", German Patent 3942205 (Feb. 1).

[7] Yang, B. et al. 2015, "High efficiency solar panel", US Patent 14/563,867 (Apr. 2).

[8] Morad, R. et al. 2016, "Shingled solar cell module", US Patent 14/605,695 (Nov. 1).

[9] Morad, R. et al., "Shingled solar cell module", US Patent 14/572,206 (Jul. 26).

[10] Morad, R. et al. 2016, "Shingled solar cell module", US Patent 14/594,439 (Jul. 19).
[11] Zhao, J. et al. 1997, "20000 PERL silicon cells for the '1996 World Solar Challenge' solar car race", *Prog. Photovolt: Res. Appl.*, Vol. 5, No. 4, pp. 269–276.
[12] Glunz, S.W. et al. 2002, "High-efficiency silicon solar cells for low-illumination applications", *Proc. 29th IEEE PVSC*, New Orleans, Louisiana, USA, pp. 450–453.
[13] Beaucarne, G. 2016, "Materials challenge for shingled cells interconnection", *Energy Procedia*, Vol. 98, pp. 115–124.
[14] SunPower Corporation 2017, "SunPower introduces new solar panel: The performance series" [https://us.sunpower.com/blog/2015/11/12/sunpower-introduces-performance-series-solar-panel/].
[15] ITRPV 2017, "International technology roadmap for photovoltaic (ITRPV): 2016 results", 8th edn (Mar.) [http://www.itrpv.net/Reports/Downloads/].
[16] Kopecek, R. & Libal, J. 2017, "Quo vadis bifacial PV?", *Photovoltaics International*, 35th edn.
[17] Blakers, A.W. et al. 1989, "22.8% efficient silicon solar cell", *Appl. Phys. Lett.*, Vol. 55, No. 13, pp. 1363–1365.
[18] Zhao, J., Wang, A. & Green, M.A. 2001, "24.5% efficiency PERT silicon solar cells on SEH MCZ substrates and cell performance on other SEH CZ and FZ substrates", *Sol. Energy Mater. Sol. Cells*, Vol. 66, Nos. 1–4, pp. 27–36.
[19] Wang, A., Zhao, J. & Green, M.A. 1990, "24% efficient silicon solar cells", *Appl. Phys. Lett.*, Vol. 57, No. 6, pp. 602–604.
[20] Norouzi, M.H. et al. 2017, "Development and characterization of multifunctional PassDop layers for local p+-laser doping", *Energy Procedia* [forthcoming].
[21] Norouzi, M.H. et al. 2017, "Development and characterization of AlO_x/SiNx:B layer systems for surface passivation and local laser doping", *IEEE J. Photovolt.* [forthcoming]
[22] Suwito, D. et al. 2010, "Industrially feasible rear passivation and contacting scheme for high-efficiency n-type solar cells yielding a V_{oc} of 700 mV", *IEEE Trans. Electron Dev.*, Vol. 57, No. 8, pp. 2032–2036.
[23] Wolf, S.D. et al. 2012, "High-efficiency silicon heterojunction solar cells: A review", *Green*, Vol. 2, No. 1.
[24] Feldmann, F. et al. 2014, "Passivated rear contacts for high-efficiency n-type Si solar cells providing high interface passivation quality and excellent transport characteristics", *Sol. Energy Mater. Sol. Cells*, Vol. 120, pp. 270–274.
[25] Fell, A., Schubert, M.C. & Glunz, S.W. 2017, "The concept of skins for (silicon) solar cell modelling", *Sol. Energy Mater. Sol. Cells* [forthcoming].
[26] Biro, D. et al. 2006, "PV-TEC: Photovoltaic technology evaluation center – Design and implementation of a production research unit", *Proc. 21st EU PVSEC*, Dresden, Germany, pp. 621–624.
[27] Werner, S. et al. 2017, "Key aspects for fabrication of p-type Cz-Si PERC solar cells exceeding 22% conversion efficiency", *Proc. 33rd EU PVSEC*, Amsterdam, The Netherlands.
[28] Saint-Cast, P. et al. 2016, "Analysis and outlook of near-industrial PERC solar cells", *Photovoltaics International*, 34th edn, pp. 52–59.
[29] Saint-Cast, P. et al. 2017, "Analysis of the losses of industrial-type PERC solar cells", *physica status solidi (a)*, Vol. 214, No. 3, p. 1600708.
[30] Hezel, R. & Jaeger, K. 1989, "Low-temperature surface passivation of silicon for solar cells", *J. Electrochem. Soc.*, Vol. 136, No. 2, pp. 518–523.
[31] Aberle, A.G. & Hezel, R. 1997, "Progress in low-temperature surface passivation of silicon solar cells using remote-plasma silicon nitride", *Prog. Photovolt: Res. Appl.*, Vol. 5, No. 1, pp. 29–50.
[32] Hübner, A., Aberle, A.G. & Hezel, R. 1997, "20% efficient bifacial silicon solar cells", *Proc. 14th EU PVSEC*, Barcelona, Spain, pp. 92–95.
[33] Krauß, K. et al. 2016, "biPERC silicon solar cells enabling bifacial applications for industrial solar cells with passivated rear sides", *physica status solidi (a)*, Vol. 213, No. 1, pp. 68–71.
[34] Wöhrle, N. et al. 2017, "Understanding the rear-side layout of p-doped bifacial PERC solar cells with simulation driven experiments", *Energy Procedia* [forthcoming].
[35] Dullweber, T. et al. 2016, "PERC+: Industrial PERC solar cells with rear Al grid enabling bifaciality and reduced Al paste consumption", *Prog. Photovolt: Res. Appl.*, Vol. 24, No. 12, pp. 1487–1498.
[36] Fellmeth, T. et al. 2017, "Co-diffused bi-facial PERT solar cells", *Energy Procedia* [forthcoming].
[37] Meier, S. et al. 2017, "Fast co-diffusion process for bifacial n-type solar cells", *Solar RRL*, Vol. 1, No. 1, p. 1600005.
[38] Meier, S. et al. 2016, "Co-diffusion for p-type PERT solar cells using APCVD BSG layers as boron doping source", *Proc. 32nd EU PVSEC*, Munich, Germany.
[39] Lohmüller, E. et al. 2017, "Bifacial p-type PERL solar cells with screen-printed pure Ag metallization and 89% bifaciality", *Proc. 33rd EU PVSEC*, Amsterdam, The Netherlands.
[40] Adachi, D., Hernández, J.L. & Yamamoto, K. 2015, "Impact of carrier recombination on fill factor for large area heterojunction crystalline silicon solar cell with 25.1% efficiency", *Appl. Phys. Lett.*, Vol. 107, No. 23, p. 233506.
[41] Strahm, B. 2017, "Heterojunction solar cells", 7th nPV worksh., Freiburg, Germany.
[42] Benick, J. et al. 2017, "High-efficiency multicrystalline n-type silicon solar cells", *Energy Procedia* [forthcoming].
[43] Röth, J. et al. 2015, "Thermal laser separation (TLS) dicing process study – A new technology for cutting silicon solar cells for high-efficiency half-cell modules", *Proc. 31st EU PVSEC*, Hamburg, Germany.
[44] Eiternick, S. et al. 2015, "High quality half-cell processing using thermal laser separation", *Energy Procedia*, Vol. 77, pp. 340–345.
[45] Lewke, D. 2015, "Thermal laser separation – TLS: Wafer-dicing der Zukunft" [www.iisb.fraunhofer.de/content/dam/iisb2014/en/Documents/events/jahrestagung-2015/jt-2015-lewke.pdf].
[46] Saint-Cast, P. et al. 2010, "High-efficiency c-Si solar cells passivated with ALD and PECVD aluminum oxide", *IEEE Electron Device Lett.*, Vol. 31, No. 7, pp. 695–697.

[47] Dicker, J. 2003, "Analyse und Simulation von hocheffizienten Silizium-Solarzellenstrukturen für industrielle Fertigungstechniken" (in German), Dissertation, Faculty of Physics, University of Konstanz, Germany.

[48] Fell, A. et al. 2017, "A detailed analysis of edge related losses in half-cells", *Proc. 33rd EU PVSEC,* Amsterdam, The Netherlands.

[49] Cuevas, A. et al. 2015, "Skin care for healthy silicon solar cells", *Proc. 42nd IEEE PVSC*, New Orleans, Louisiana, USA, pp. 1–6.

[50] SunPower Corp, "SunPower Performance Series P17: Technical product datasheet".

[51] Zhao, J. et al. 1997, "Improved efficiency silicon solar cell module", *IEEE Electron Device Lett.*, Vol. 18, No. 2, pp. 48–50.

[52] Mittag, M. 2017, "Systematic PV-module optimization with the cell-to-module (CTM) analysis software 'SmartCalc.CTM'", *Photovoltaics International,* 36th edn.

[53] Mittag, M. "Cell-to-Module (CTM) Analysis for photovoltaic modules with shingled solar cells", *Proc. 44th IEEE PVSC,* Washington DC, USA.

[54] Mittag, M. 2017, "Progress on unified cell-to-module (CTM) determination methodology: Systematic calculation of module power", *Proc. 44th IEEE PVSC,* Washington DC, USA.

[55] Clover, I. 2016, "Trina Solar sets new 22.61% mono PERC efficiency record", *pv magazine* (Dec.).

About the Authors

Nico Wöhrle studied physics at the University of Freiburg, Germany, and was awarded his diploma degree in 2012 for his work at Fraunhofer ISE on the optical simulation of silicon solar cells. He received his Ph.D. from the University of Freiburg in 2016, with a topic involving the simulation of PERC solar cells. He is currently a researcher at Fraunhofer ISE, where he focuses on the simulation and modelling of solar cells, as well as on the conceptual development of p-type PERC solar cells.

Elmar Lohmüller studied physics at the University of Tübingen, Germany, and at Nelson Mandela Metropolitan University, Port Elizabeth, South Africa. He received his diploma degree in 2010 for his work at Fraunhofer ISE on the development of p-type MWT-PERC solar cells, followed by his Ph.D. from the University of Freiburg in 2015 for his contributions to the development of n-type MWT solar cells. He is currently a researcher at Fraunhofer ISE, with a focus on the development of p-type PERC solar cells.

Max Mittag studied industrial engineering and management at the Freiberg University of Mining and Technology. In 2010 he completed his diploma thesis at Fraunhofer ISE and joined the PV module department. His current work includes CTM efficiency analysis and the development of new PV module concepts.

Anamaria Moldovan studied chemistry at the University of Zurich, Switzerland, and in Freiburg, Germany, receiving her diploma degree in 2011 for her work at Fraunhofer ISE on wet chemical cleaning. She was awarded her Ph.D. by the University of Freiburg in 2016 for her investigations of cleaning and conditioning for high-efficiency silicon solar cells. She is currently a researcher at Fraunhofer ISE, focusing on the development of wet chemical and plasma processes for solar cells with passivated contacts.

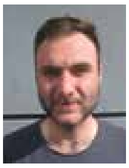

Puzant Baliozian obtained a B.Sc. in physics in 2014 from the American University of Beirut. In 2016 he received his M.Sc. in renewable energy engineering and management from the University of Freiburg for his thesis work completed at Fraunhofer IPM in the field of magnetocaloric energy conversion. He is currently a Ph.D. candidate at Fraunhofer ISE, where his main area of research is the development of p-type SPEER solar cells.

Tobias Fellmeth studied physics at the University of Konstanz, Germany, and received his diploma degree in 2009 for his work at Fraunhofer ISE on the development and characterization of MWT concentrator solar cells. He was awarded his Ph.D. by the University of Tübingen in 2014 for his studies of silicon-based, low-concentrator solar cells. He is currently a scientist at Fraunhofer ISE, where he focuses on the development of bifacial p-type PERC solar cells.

Karin Krauss studied physics at the Albert Ludwig University of Freiburg and received her diploma degree in 2012. Since 2013 she has been working towards her Ph.D. at Fraunhofer ISE. She joined the PV production technology and quality assurance division at Fraunhofer ISE in 2011, where her research interests involve multicrystalline silicon solar cells and light-induced degradation.

Achim Kraft studied electrical engineering at the University of Applied Science in Hanover, Germany, and renewable energies at the University of Applied Science in Berlin. He received his master's in renewable energies, before joining Fraunhofer ISE in 2012 as a Ph.D. student. He was awarded his Ph.D. in the field of plated-copper front-side metallizations for silicon solar cells by the Albert Ludwig University of Freiburg in 2015. Since then he has focused on solar cell interconnection technologies and processes as head of the interconnection technologies team in the module research group at Fraunhofer ISE.

Ralf Preu is director of the PV production technology division at Fraunhofer ISE in Freiburg, Germany, and also teaches PV at the University of Freiburg. He studied physics at the Universities of Freiburg and Toronto, and economics at the University of Hagen, Germany. He holds a Ph.D. in electrical engineering, and joined Fraunhofer ISE in 1993. His work in different fields in PV includes system monitoring, and silicon solar cell and module technology, characterization and simulation, but his main focus is R&D in advanced silicon solar cell technology and its transfer to industrial production.

Enquiries

Nico Wöhrle
Fraunhofer Institute for Solar Energy Systems ISE
Heidenhofstraße 2
79110 Freiburg, Germany

Tel: +49 (0)761 4588 5964
Email: nico.woehrle@ise.fraunhofer.de